Published in final edited form as:
*Nano Lett*. 2012 July 11; 12(7): 3437–3442. doi:10.1021/nl300673r.

# Voltage-gated ion transport through semiconducting conical nanopores formed by metal nanoparticle assisted plasma etching

**Teena James**[1], **Yevgeniy V. Kalinin**[1], **Chih-Chieh Chan**[1], **Jatinder S. Randhawa**[1], **Mikhail Gaevski**[3], and **David H. Gracias**[1,2]

David H. Gracias: dgracias@jhu.edu

[1]Department of Chemical and Biomolecular Engineering, Johns Hopkins University, Baltimore, MD 21218, USA

[2]Department of Chemistry, Johns Hopkins University, Baltimore, MD 21218, USA

[3]Princeton Institute for the Science and Technology of Materials, Princeton University, Princeton, NJ 08540, USA

## Abstract

Nanopores with conical geometries have been found to rectify ionic current in electrolytes. While nanopores in semiconducting membranes are known to modulate ionic transport through gated modification of pore surface charge, the fabrication of conical nanopores in silicon (Si) has proven challenging. Here, we report the discovery that gold (Au) nanoparticle (NP) assisted plasma etching results in the formation of conical etch profiles in Si. These conical profiles result due to enhanced Si etch rates in the vicinity of the Au NPs. We show that this process provides a convenient and versatile means to fabricate conical nanopores in Si membranes and crystals with variable pore-diameters and coneangles. We investigated ionic transport through these pores and observed that rectification ratios could be enhanced by a factor of over 100 by voltage gating alone, and that these pores could function as ionic switches with high on-off ratios of approximately 260. Further, we demonstrate voltage gated control over protein transport, which is of importance in lab-on-a-chip devices and biomolecular separations.

### Keywords

nanofluidics; membranes; separations; ion channels; ionic circuits; electrochemistry

Solid-state nanopores have attracted a great deal of scientific interest due to their possible use in replicating some behaviors observed in naturally occurring trans-membrane protein channels[1–3]. In order to mimic the complex chemo-electrical control that is observed in protein channels[4, 5], there is a need to incorporate mechanisms for active control of ion transport through solid state nanopores[6, 7]. Nanopores formed in semiconducting substrates such as silicon (Si) offer the possibility for voltage-gated control of transmembrane ionic and molecular transport[8, 9]. Furthermore, nanopores in Si membranes are mechanically robust, biocompatible, able to tolerate a wide variety of environmental conditions and permit facile integration with existing Si-based electronic and micromechanical devices[10]. When considering the effect of geometry on nanopore transport characteristics, conical nanopores have been found to exhibit unique ion transport properties as a consequence of their

Correspondence to: David H. Gracias, dgracias@jhu.edu.

asymmetric geometry[11]. For example, the ionic rectification behavior observed in conical nanopores, due to surface charge density asymmetry[12], can be utilized to develop ionic analogs of electronic devices[13, 14]. Further, for nanopores of conical geometry exhibit lower electrical resistance in comparison to those with cylindrical geometries of the same tip diameter, making them more suitable for molecular sensing applications, as these pores generate higher ionic currents[15]. Hence, conical nanopores in semiconducting substrates are attractive for a wide range of applications including the creation of synthetic analogous of biological nanochannels[16], ionic logic circuitry[17, 18] and actively controllable molecular separation platforms[19]. However, the generation of conical nanopores in single crystal Si, to enable gated, active control, is challenging using existing methodologies.

There exist a variety of methods to create nanopores. These include the widely utilized track etching method, which enables the creation of conical nanopores in polymeric thin films through ion bombardment and subsequent chemical etching[12]. However, this method is restricted to homogenous dielectrics and also requires the use of MeV to GeV ion sources[20]. Although wet chemical etching of e-beam lithography patterned Si has been used to form nanopores, it offers limited control over the pore geometry in terms of cone angles and often results in faceted pores due to the varying etch rates along the different Si crystallographic planes[21–24]. Here, we describe the process of nanopore formation in Si substrates, that relies on an enhancement of the dry etch rate observed in the presence of Au nanoparticles (NPs)[25]. The process can be implemented in a maskless manner and does not require lithographic patterning. Further, the etch process allows considerable control over pore geometry and the application of a voltage to nanoporous Si membranes enables active control over small ion and protein transport.

We discovered that $CF_4$-$O_2$ plasma etching of single crystal Si substrates in the vicinity of Au NPs resulted in a conical etch profile (Figure 1). In order to characterize the process, we utilized silicon on insulator (SOI) wafers with different Si device layer thicknesses. We first dispersed Au NPs on the surface of the Si device layer and then plasma etched and released the Si membranes by dissolving the buried oxide layer in hydrofluoric acid (HF) (Figure 2a and details in supporting information). It is also noteworthy that this process is versatile in that Au NPs can also be dispersed on flexible Si membranes or Si powder crystals so that such conical nanopores can be formed on these substrates (Figure 2b–d). While dispersal of NPs can be used to form conical nanopores in a lithography-free manner, our process is also compatible with lithographically defined Au patterns which may be required in applications that require precise positioning or ordered arrays of nanopores. We were able to utilize both e-beam lithography to pattern individual Au discs which could be plasma etched to form precisely positioned isolated nanopores as well as nanoimprint lithography (NIL) to define arrays of Au nano-discs (Figure 2e), which could also be plasma etched to create large-area ordered nanopore arrays in Si membranes (Figure 2f).

In order to optimize the etching conditions, we first explored the effects of varying $CF_4/O_2$ ratio on bare Si wafers and observed that a ratio of 25 sccm $CF_4$ and 4 sccm $O_2$ resulted in optimum etching (details in supporting information). Further, we estimate that the Au NPs enhance the etch rate of Si by over an order of magnitude, with measured increases in Si etch rate from ~110 nm/min to as high as ~4000 nm/min, and the etch rate was sensitive to the type of etcher used and the density of the nanoparticles. It is noteworthy that enhancements in wet etching rates of Si have been observed using a metal assisted chemical etching (MaCE) process[26, 27]. In the MaCE process, the Si substrate with a noble metal mask is wet etched with hydrofluoric acid (HF) and an oxidative agent, typically hydrogen peroxide ($H_2O_2$). During etching, the Si beneath the noble metal is etched much faster than the uncovered Si. The enhanced etching of Si at the Si/metal interface has been attributed to

preferential reduction of the oxidant at the surface of the noble metal with associated hole injection into the Si[26, 28].

In contrast, our mechanism for the formation of conical etch-profiles is based on the accelerated dry etching of Si in the vicinity of Au NPs[25]. It has been shown that the presence of Au or its oxide increases the etch rate of Si in $CF_4$-$O_2$ plasma[29]; this acceleration has been attributed to a metal-catalyzed increase in the concentration of reactive fluorine radicals (F*)[30, 31]. We developed a theoretical model (details in supporting information) that captures the effects of an enhanced etch rate in the vicinity of the Au NP and predicts a conical etch profile (Figure 3a). From the model, the cone half-angle (θ) can be related to the etch rates and etch anisotropy (*k*) as,

$$\theta = \arctan\left[\frac{1}{k\sqrt{(v_1/v_0)^2 - 1}}\right] \quad \text{(Equation 1)}$$

Experimentally, we varied the etch power and found that higher RF powers generated wider cone angles (Figure 3b; results in supporting information). We observed that the conical tip radii of nanopores formed using Au NPs of 50 nm diameter were smaller than those formed using 100 nm particles and that the radii increased linearly with time (Figure 3c). The smallest pore diameter that we have reproducibly achieved is around 20 nm. Since the etch rate of Si is rapid, reproducible formation of even smaller pores would require further optimization in terms of tuning the etch rate as well as the Si device layer thickness.

We characterized the NP dispersed Si surface after plasma etching using Fourier Transform Infra-Red (FTIR) spectroscopy, X-Ray Photoelectron Spectroscopy (XPS) and contact angle measurements (details in supporting information). Our characterization studies suggest that the Si surface is coated with a dielectric layer, about 1.5 nm thick, composed largely of oxidized silicon. Such oxidized Si surfaces (pI ~ 2) are known to exhibit a negative surface charge when in contact with aqueous electrolyte solutions of pH > 3 due to de-protonation of the Si-OH surface groups (pKa ~ 6.9)[32, 33].

In order to explore the use of these conical nanopores in the creation of bio-mimetic ion channels, we measured the transmembrane current across a single plasma etched nanopore (Figure 4). The nanopore was fabricated in a 20 μm thick Si device layer with a pore base and tip diameter of approximately 2.5 μm and 43 nm respectively (Figure 4a, see supporting information for fabrication details). We attribute the origin of the observed rectification to the conical asymmetric geometry and the negative charge present on the pore surface[13, 34–36] (Figure 4b). In addition, we observed that the rectification ratio (*f*) decreased from 3.9 to 2.3 when the KCl electrolyte concentration increased from 20 mM to 100 mM (Figure 4c). We rationalize this observation by noting that theoretical predictions based on Poisson-Nernst-Planck equations suggest that rectification occurs when the electrical double layer widths become comparable to the charged conical nanopore dimensions[37–39]. As the concentration of the electrolyte and consequently ionic strength increases, the double layer width decreases relative to the pore size and hence the pore becomes a less effective rectifier[36, 37]. Further, at a fixed electrolyte concentration of 20 mM KCl, we observed that the rectification ratio also varied with pH (Figure 4d). Significantly, the rectification ratio was found to decrease from $f = 4.2$ at pH 8 to $f = 1.1$ at pH 2, indicating that the surface charge of the pore walls play a major role in the rectification behavior. The low degree of rectification at low pH is indicative of the neutralization of the negative surface charges present on the pore wall, due to protonation. Such a pH sensitive behavior of Electrolyte Insulator Semiconductor (EIS) systems consisting of Si, oxidized silicon and aqueous

electrolyte have been well previously described in the context of Ion Selective Field Effect Transistors (ISFETs)[33, 40].

One significant advantage of semiconducting conical nanopores is that the space charge at the semiconductor interface can be manipulated by the application of a voltage. We measured the *I-V* characteristics of transmembrane ionic transport in 20 mM KCl and observed a variation in the ionic current as a function of the voltage applied to the Si membrane (Figure 5). Using a transistor analogy, we plotted the ionic current ($I_D$) as a function of drain voltage ($V_D$) for a fixed gate voltage ($V_G$) (Figure 5c). In contrast to manipulating transmembrane ion transport by varying the size, shape or surface charge of the pore using various strategies such as thiolated DNA molecules[41], polyelectrolyte deposition[42] and pH responsive polymer brushes[43, 44], we observe that active control can be achieved by voltage gating. We found the variation to be more pronounced at negative $V_G$. For example, at $V_G = -2$ V, $I_D$ was increased by a factor of six as compared to that when no gate voltage was applied, while there was a negligible effect at positive voltages, as expected. We rationalize this result by noting that increasing the negative gate bias on the Si enhances the negative space charge within the semiconducting Si surface (as verified by Kelvin probe microscopy; details in supporting information) resulting in higher transport rate of K+ ions through the more negatively charged pore.

We note that this non-linear *I-V* behavior can be used to enable ionic switching (ON/OFF) devices (Figure 5d) of relevance to ionic logic circuitry. Here, a square wave pulse of amplitude −2 V to +2 V was applied to the gate electrode and the transmembrane current was measured. The nanopore device was found to continuously switch between ON and OFF states at negative gate bias (−2 V) and positive gate bias (+2 V) respectively (Figure 5e). We attribute the high noise in the ON state of the device to the combined effects of fluctuations in the pore surface charge, dynamic electrowetting phenomena in the porewall and the thermal fluctuations in the conductivity of the salt solution[45–49]. We estimate that the rectification ratios in our devices could be readily varied across two orders of magnitude by voltage gating alone and the ionic switching measurement revealed an ionic current on/off ratio of approximately 260. Thus, analogous to biological membranes, active control over transmembrane ion transport can be achieved by the application of electric potential to Si nanoporous membrane.

In addition to gate modulated rectification properties of small ions, we observed that active control over permeation of charged biomolecules can also be achieved through semiconducting nanoporous membranes, which is important in lab-on-a-chip devices and biomolecular separations[50]. We studied the time dependent permeation of fluorescently labeled Bovine Serum Albumin (BSA) molecules through an approximately 4 mm diameter nanoporous region of the membrane with and without the application of a voltage (Figure 6a) (see supporting information for details). Importantly, as shown in the plot of fluorescence intensity with time (Figure 6b), we observed significantly enhanced transport at +0.3 V bias as compared to that at 0 V and −0.3 V. We attribute this change to electrostatic effects of the negatively charged BSA (pI 4.7), and enhanced diffusion at positive voltages. In order to estimate the significance of this difference, we developed a transport model (details in supporting information) which suggests that this difference is equivalent to an increase in the effective diffusion coefficient of BSA by over an order of magnitude when either +0.3 V or −0.3 V is applied.

In summary, we have uncovered a convenient and versatile process to form conical nanopores in semiconducting, single crystal Si substrates. The process is simple, can be utilized in a maskless, lithography free manner which increases its accessibility. Additionally, semiconducting nanopores allow facile control over transmembrane ionic and

molecular transport and it is conceivable that the incorporation of gate dielectrics could enable ionic field effect transistors. Since the process is versatile and compatible with MEMS / CMOS processes, these voltage gated ionic devices could be integrated with electronic and micromechanical structures.

## Supplementary Material

Refer to Web version on PubMed Central for supplementary material.

## Acknowledgments

This work was supported by the NSF CMMI 0854881 and the NIH Director's New Innovator Award Program, part of the NIH Roadmap for Medical Research, through grant number DP2-OD004346-01. Information about the NIH Roadmap can be found at http://nihroadmap.nih.gov. We are grateful to George P. Watson and Joseph Palmer of PRISM (Princeton Institute for the Science and Technology of Materials) clean room facility for their help with device fabrication and valuable discussions. We acknowledge technical assistance and suggestions from Gary Johns, Nina Markovic, Michael Barclay, Howard Fairbrother and Joyce Breger. We also acknowledge use of the Surface Analysis lab at JHU (Department of Materials Science and Engineering).

## References

1. Dekker C. Nat. Nanotechnol. 2007; 2(4):209–215. [PubMed: 18654264]
2. Hou X, Guo W, Jiang L. Chem. Soc. Rev. 2011; 40(5):2385–2401. [PubMed: 21308139]
3. Jovanovic-Talisman T, Tetenbaum-Novatt J, McKenney AS, Zilman A, Peters R, Rout MP, Chait BT. Nature. 2009; 457(7232):1023–1027. [PubMed: 19098896]
4. Majd S, Yusko EC, Billeh YN, Macrae MX, Yang J, Mayer M. Curr. Opin. Biotechnol. 2010; 21(4): 439–476. [PubMed: 20561776]
5. Sigworth FJ. Nature. 2003; 423(6935):21–22. [PubMed: 12721605]
6. Karnik R, Castelino K, Fan R, Yang P, Majumdar A. Nano Lett. 2005; 5(9):1638–1642. [PubMed: 16159198]
7. Siwy ZS, Howorka S. Chem. Soc. Rev. 2010; 39(3):1115–1132. [PubMed: 20179828]
8. Gracheva ME, Vidal J, Leburton J-P. Nano Lett. 2007; 7(6):1717–1722. [PubMed: 17516680]
9. Vidal J, Gracheva ME, Leburton JP. Nanoscale. Res. Lett. 2007; 2(2):61–68.
10. van den Berg A, Wessling M. Nature. 2007; 445(7129):726–726. [PubMed: 17301783]
11. Sexton LT, Horne LP, Martin CR. Mol. BioSyst. 2007; 3(10):667–685. [PubMed: 17882330]
12. Apel PY, Korchev YE, Siwy Z, Spohr R, Yoshida M. Nucl. Instrum. Methods Phys. Res. Sect. B. 2001; 184(3):337–346.
13. Zhou K, Perry JM, Jacobson SC. Annu. Rev. Anal. Chem. 2011; 4:321–341.
14. Guan W, Fan R, Reed MA. Nat. Commun. 2011; 2:506. [PubMed: 22009038]
15. Mara A, Siwy Z, Trautmann C, Wan J, Kamme F. Nano Lett. 2004; 4(3):497–501.
16. Martin CR, Siwy ZS. Science. 2007; 317(5836):331–332. [PubMed: 17641190]
17. Zhong C, Deng Y, Roudsari AF, Kapetanovic A, Anantram MP, Rolandi M. Nat. Commun. 2011; 2:476. [PubMed: 21934660]
18. Mafe S, Manzanares JA, Ramirez P. J. Phy. Chem. C. 2010; 114(49):21287–21290.
19. Kovarik ML, Jacobson SC. Anal. Chem. 2009; 81(17):7133–7140. [PubMed: 19663470]
20. Spohr R. Radiat. Meas. 2005; 40(2–6):191–202.
21. Storm AJ, Chen JH, Ling XS, Zandbergen HW, Dekker C. Nat. Mater. 2003; 2(8):537–540. [PubMed: 12858166]
22. Striemer CC, Gaborski TR, McGrath JL, Fauchet PM. Nature. 2007; 445(7129):749–753. [PubMed: 17301789]
23. Park SR, Peng H, Ling XS. Small. 2007; 3(1):116–119. [PubMed: 17294481]
24. Bean KE. IEEE Trans. Electron. Devices. 1978; ED-25(10):1185–1193.

25. James T, Cho JH, Fernandes R, Randhawa JS, Gracias DH. Anal. Bioanal. Chem. 2010; 398(7–8): 2949–2954. [PubMed: 20936261]
26. Huang Z, Geyer N, Werner P, de Boor J, Gösele U. Adv. Mater. 2011; 23(2):285–308. [PubMed: 20859941]
27. Rykaczewski K, Hildreth OJ, Wong CP, Fedorov AG, Scott JHJ. Nano Lett. 2011; 11(6):2369–2374. [PubMed: 21526791]
28. Tsujino K, Matsumura M. Adv. Mater. 2005; 17(8):1045–1047.
29. Kataoka Y, Shinmura T, Kanoh M. J. Vac. Sci. Technol. A. 2000; 18(2):388–392.
30. Fedynyshyn TH, Grynkewich GW, Chen BA, Ma TP. J. Electrochem. Soc. 1989; 136(6):1799–1804.
31. Fedynyshyn TH, Grynkewich GW, Dumas RH. J. Electrochem. Soc. 1988; 135(1):268–269.
32. Bousse L, De Rooij NF, Bergveld P. IEEE Trans. Electron. Devices. 1983; ED-30(10):1263–1270.
33. van Hal REG, Eijkel JCT, Bergveld P. Adv. Colloid Interface Sci. 1996; 69(1–3):31–62.
34. Siwy ZS. Adv. Funct. Mater. 2006; 16(6):735–746.
35. Siwy Z, Heins E, Harrell CC, Kohli P, Martin CR. J. Am. Chem. Soc. 2004; 126(35):10850–10851. [PubMed: 15339163]
36. Liu Q, Wang Y, Guo W, Ji H, Xue J, Ouyang Q. Phys. Rev. E. 2007; 75:051201.
37. Daiguji H, Yang P, Majumdar A. Nano Lett. 2004; 4(1):137–142.
38. Cervera J, Schiedt B, Ramírez P. Europhys. Lett. 2005; 71(1):35–41.
39. Ai Y, Zhang M, Joo SW, Cheney MA, Qian S. J. Phys. Chem. C. 2010; 114(9):3883–3890.
40. Fung CD, Cheung PW, Ko WH. IEEE Trans. Electron. Devices. 1986; ED-33(1):8–18.
41. Harrell CC, Kohli P, Siwy Z, Martin CR. J. Am. Chem. Soc. 2004; 126(48):15646–15647. [PubMed: 15571378]
42. Ali M, Yameen B, Cervera J, Ramírez P, Neumann R, Ensinger W, Knoll W, Azzaroni O. J. Am. Chem. Soc. 2010; 132(24):8338–8348. [PubMed: 20518503]
43. Yameen B, Ali M, Neumann R, Ensinger W, Knoll W, Azzaroni O. J. Am. Chem. Soc. 2009; 131(6):2070–2071. [PubMed: 19159287]
44. Yameen B, Ali M, Neumann R, Ensinger W, Knoll W, Azzaroni O. Nano Lett. 2009; 9(7):2788–2793. [PubMed: 19518086]
45. Smeets RMM, Dekker NH, Dekker C. Nanotechnol. 2009; 20:9.
46. Smeets RMM, Keyser UF, Dekker NH, Dekker C. Proc. Natl. Acad. Sci. U.S. A. 2008; 105(2): 417–421. [PubMed: 18184817]
47. Wang L, Sun L, Wang C, Chen L, Cao L, Hu G, Xue J, Wang Y. J. Phys. Chem. C. 2011; 115(46): 22736–22741.
48. Hoogerheide DP, Garaj S, Golovchenko JA. Phys. Rev. Lett. 2009; 102:25.
49. Smirnov SN, Vlassiouk IV, Lavrik NV. ACS Nano. 2011; 5(9):7453–7461. [PubMed: 21838311]
50. Karnik R, Castelino K, Majumdar A. Appl. Phys. Lett. 2006; 88(12):123114/3.

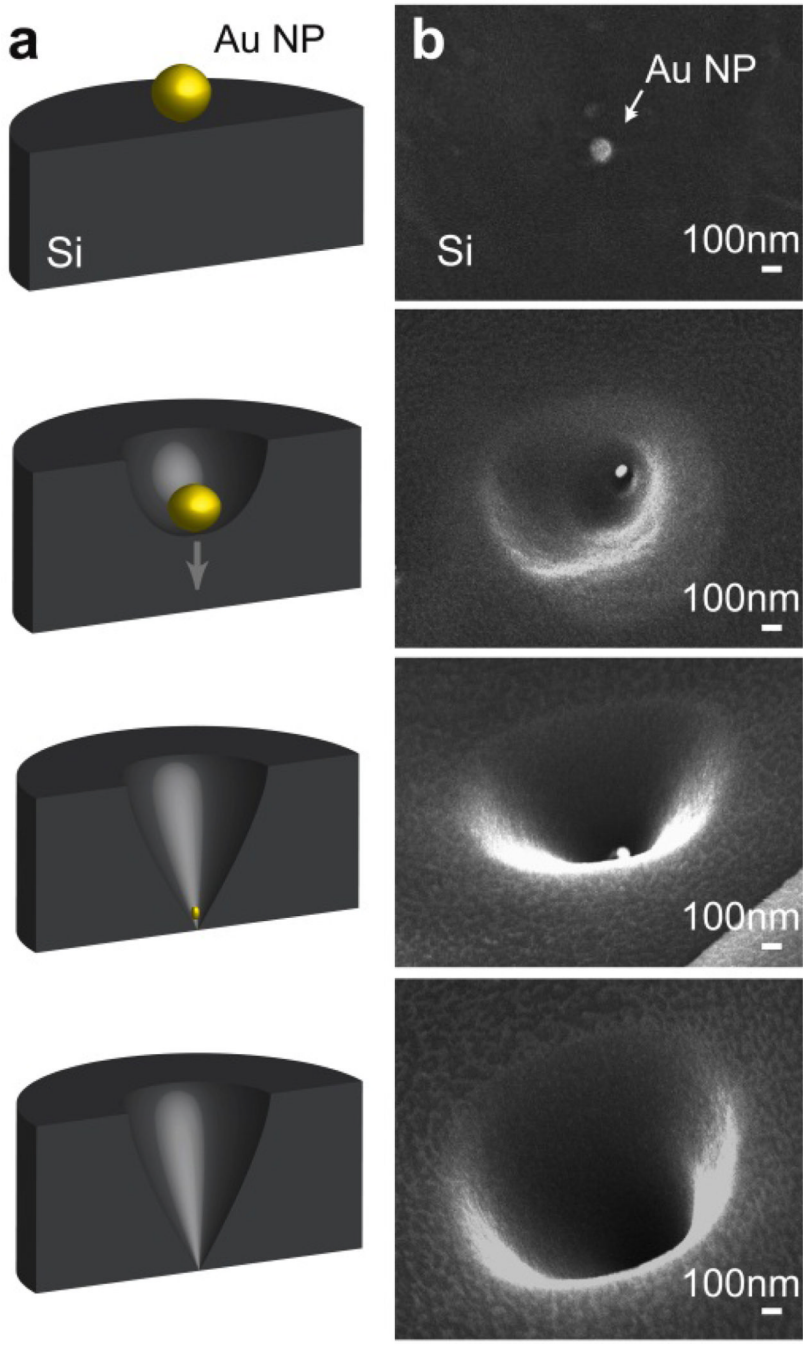


**Figure 1. Schematic illustration and corresponding SEM images of conical nanopore formation during plasma etching of a Si substrate in the vicinity of an Au NP**

(a) Schematic illustration of the process. (b) SEM images of an Au NP on the Si surface before etching and at different times during the plasma etching process.

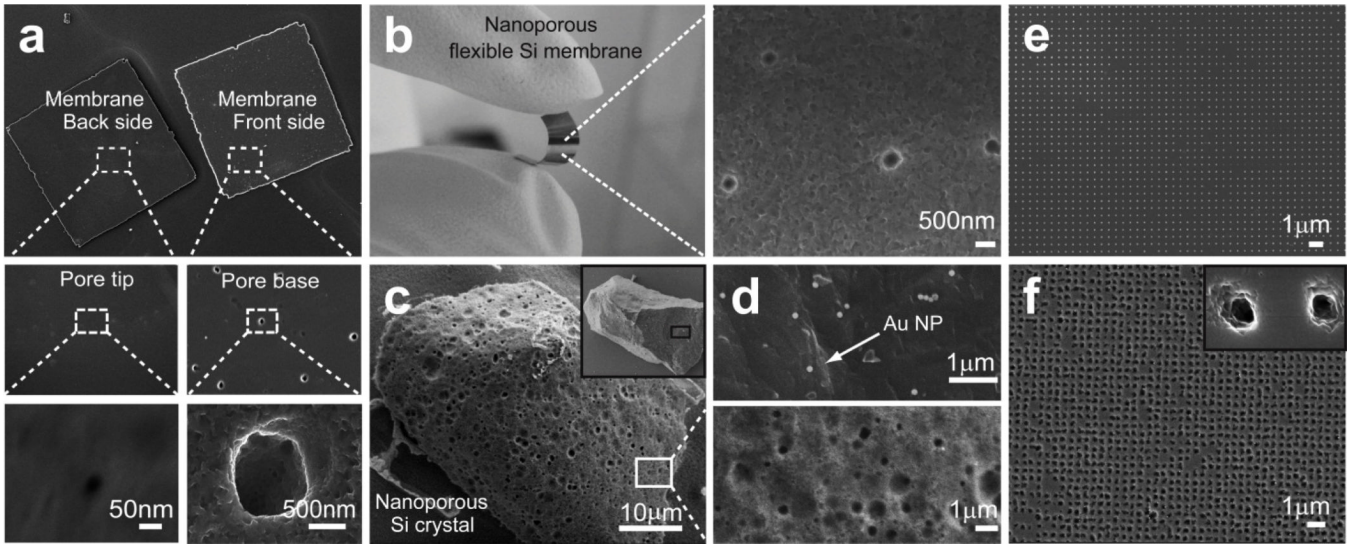


**Figure 2. Versatility of conical nanopore formation in different Si substrates**

(a) SEM images of nanoporous Si membranes (500 μm square) at different magnifications showing back-side (pore tip) and front-side (pore base). (b) Optical image of a large-area Si nanoporous membrane with nanopores evident in the SEM image (right panel) of the membrane surface. (c) Progressively zoomed-in SEM images of a nanoporous Si crystal formed by our etching process; inset shows a Si crystal with dispersed Au NPs before etching. (d) Zoomed-in SEM image of the Si surface dispersed with Au NPs before etching. (e–f) SEM images of an array of gold nanodiscs patterned using nanoimprint lithography (e) before and (f) after etching; inset shows a representative zoomed-in SEM image of the nanopores in the array.

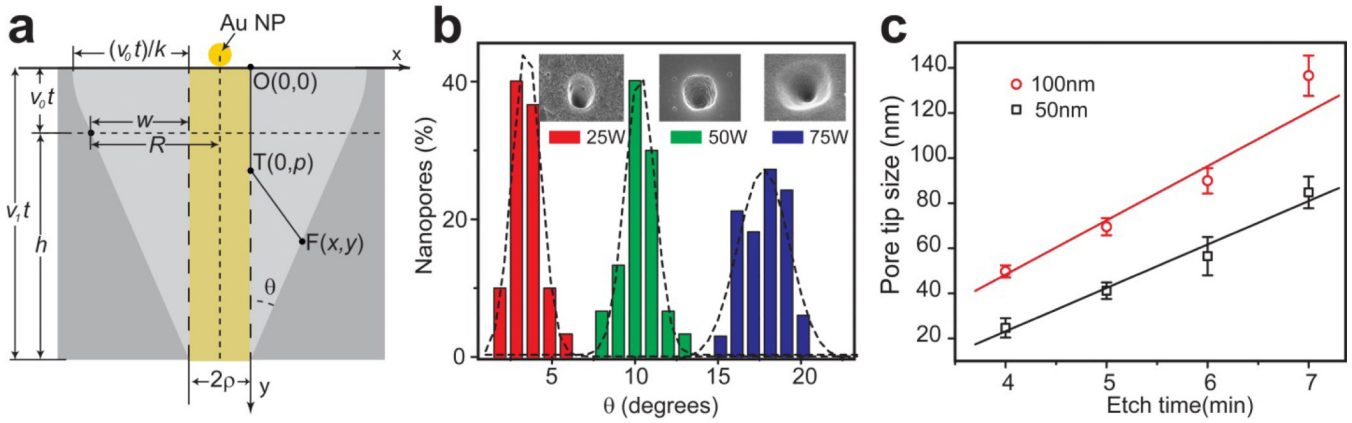


**Figure 3. Model and experimental control of nanopore cone angle and size**

(a) Illustration of our etch model for conical nanopore formation. (b) Plot of the variation of the cone half-angle with etch power (25, 50 and 75W) obtained using 100 nm Au NPs. (c) Plot of the variation of the nanopore tip size with etching time. The data was obtained using 50 nm and 100 nm diameter Au NPs (Bars indicate the standard deviation).

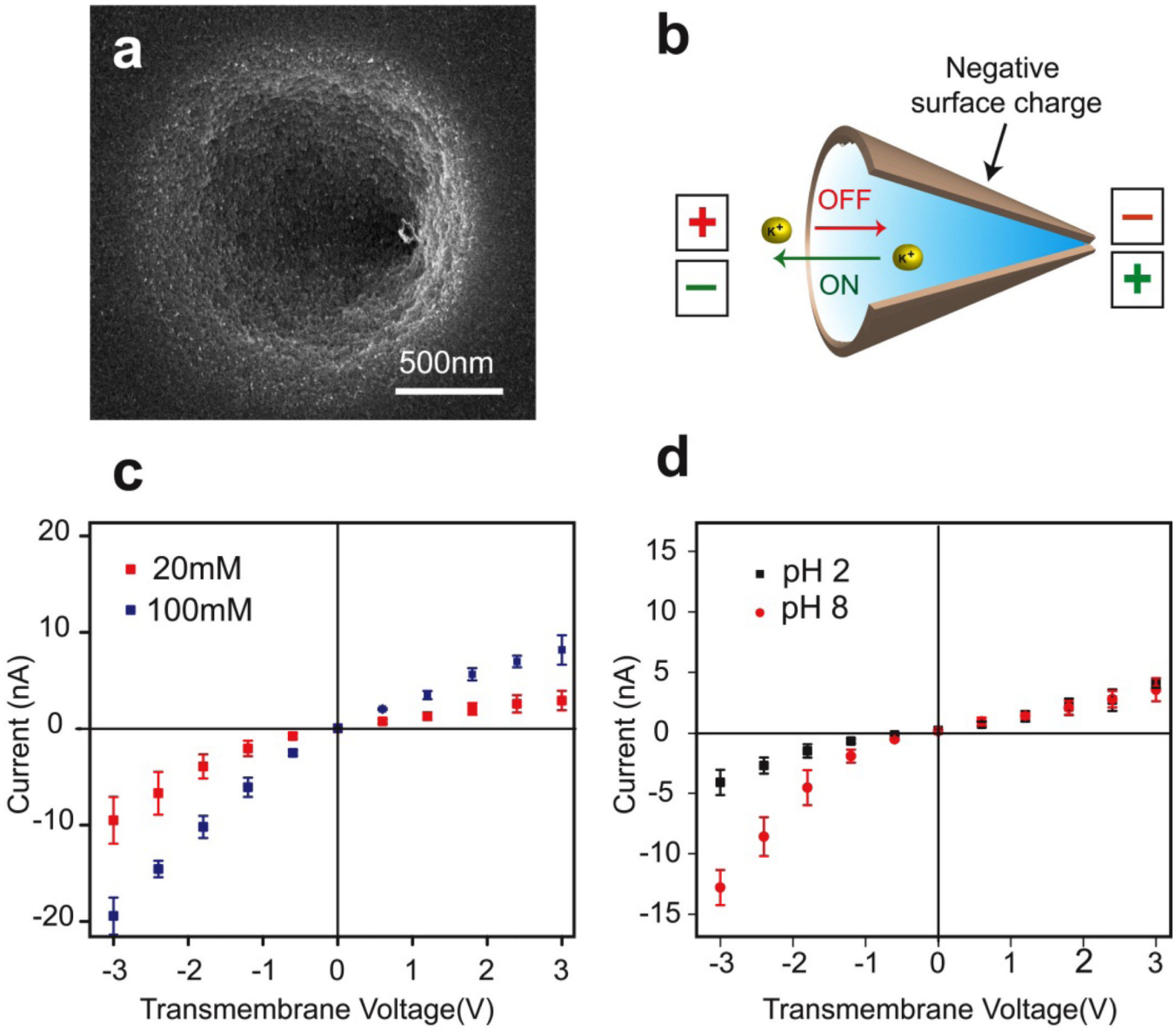


**Figure 4. Ion-current rectification observed in an individual conical nanopore**

(a) Representative SEM image of the individual conical nanopore formed by plasma etching of an e-beam patterned Au disc. (b) Illustration of ionic current rectification in a conical nanopore. The arrows illustrate the motion of cations and relative magnitude of ionic current in the corresponding electrode configurations. (c) *I-V* curves measured in 20 mM and 100 mM KCl at pH 7. (d) *I-V* curves measured in 20 mM KCl at pH 2 and pH 8 (bars indicate the standard deviation, N=3). The measurements were performed on a single conical nanopore with tip diameter of approximately 43 nm.

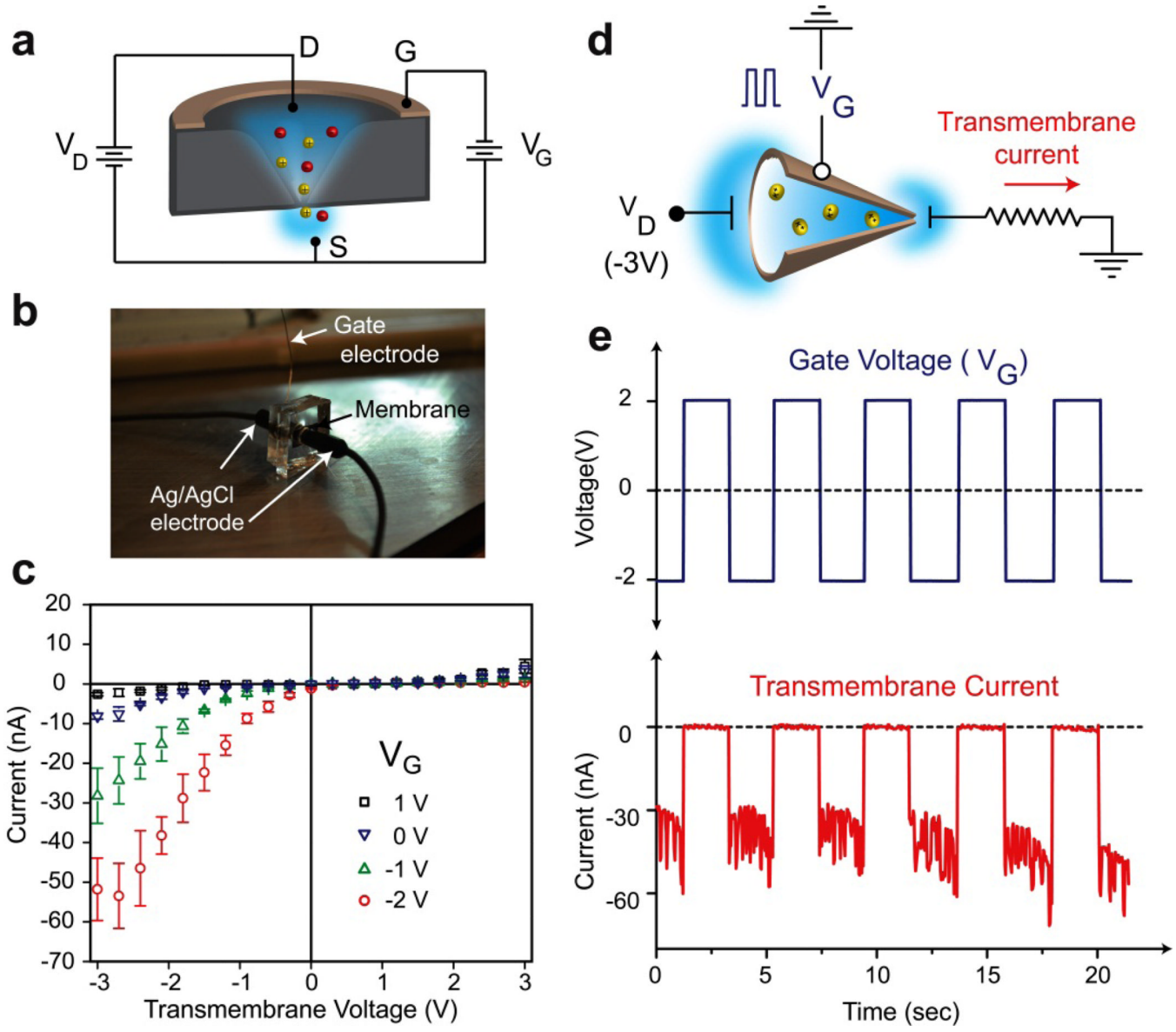


**Figure 5. Voltage-gated switching of ionic current through an individual conical nanopore**

(a) Schematic illustrating the gated ionic transmembrane transport through a Si conical nanopore. (b) Optical image of the measurement setup and (c) $I_D$-$V_D$ plot with varying VG between -2 V to 1 V. (d–e) Switching ionic circuit. (d) Schematic of the circuit used to measure the switching behavior of the conical nanopore device, and (e) switching behavior obtained by varying the gate voltage which results in synchronized transmembrane current across the load resistor. The current-voltage recordings were made with a solution of 20 mM KCl, pH 7 and the measurements were performed on a single conical nanopore with tip diameter of approximately 35 nm (bars indicate the standard deviation, N=3).

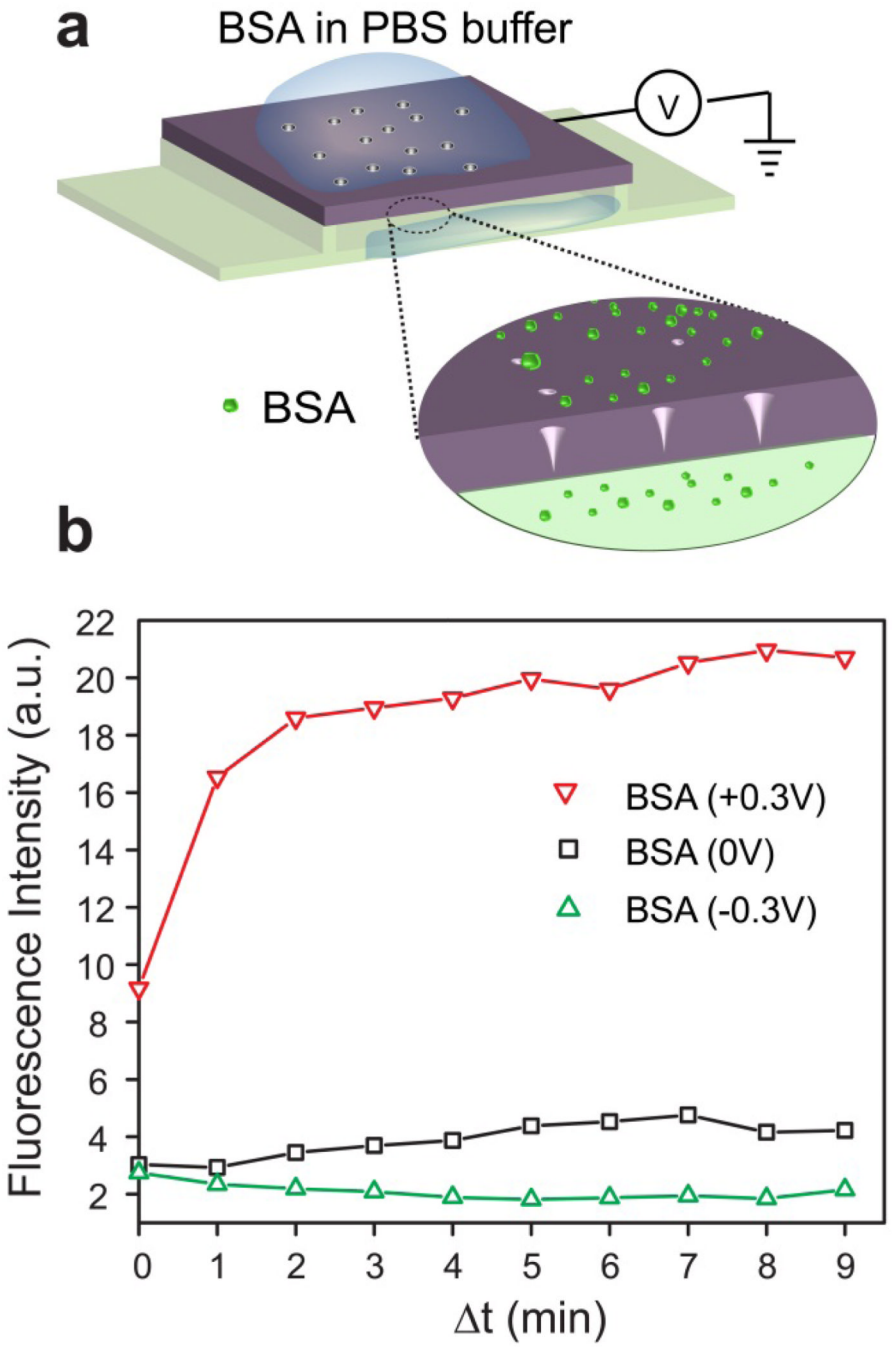


**Figure 6. Voltage control of protein transport**

(a) Schematic illustration of BSA protein transport across a nanoporous membrane, and (b) representative plot of fluorescence intensity vs. time for voltage gated (−0.3 V, 0 V, 0.3 V) transport of BSA-FITC conjugate through the membrane; Δt indicates the time from the start of observation.